Updated T2K measurements of muon neutrino and antineutrino disappearance using 3.6×10^21 protons on target

メタデータ	言語: English
	出版者: American Physical Society
	公開日: 2024-12-12
	キーワード (Ja):
	キーワード (En):
	作成者: Honjo, T., Kobata, T., Nishizaki, K., Okusawa, T., Seiya, Yoshihiro, Takayasu, S., Teshima, N., Yamamoto, Kazuhiro, Yamamoto, T., T2K Collaboration
	メールアドレス:
	所属:
URL	http://hdl.handle.net/10466/0002001452

Updated T2K measurements of muon neutrino and antineutrino disappearance using 3.6×10^{21} protons on target

K. Abe,[60] N. Akhlaq,[49] R. Akutsu,[15] A. Ali,[71,66] S. Alonso Monsalve,[10] C. Alt,[10] C. Andreopoulos,[37] M. Antonova,[19] S. Aoki,[32] T. Arihara,[63] Y. Asada,[73] Y. Ashida,[33] E. T. Atkin,[21] M. Barbi,[50] G. J. Barker,[70] G. Barr,[46] D. Barrow,[46] M. Batkiewicz-Kwasniak,[14] F. Bench,[37] V. Berardi,[22] L. Berns,[69] S. Bhadra,[74] A. Blanchet,[12] A. Blondel,[57,12] S. Bolognesi,[5] T. Bonus,[72] S. Bordoni,[12] S. B. Boyd,[70] A. Bravar,[12] C. Bronner,[60] S. Bron,[66] A. Bubak,[56] M. Buizza Avanzini,[36] J. A. Caballero,[54] N. F. Calabria,[22] S. Cao,[20] D. Carabadjac,[36,*] A. J. Carter,[52] S. L. Cartwright,[55] M. P. Casado,[17] M. G. Catanesi,[22] A. Cervera,[19] J. Chakrani,[36] D. Cherdack,[16] P. S. Chong,[47] G. Christodoulou,[11] A. Chvirova,[26] M. Cicerchia,[24,†] J. Coleman,[37] G. Collazuol,[24] L. Cook,[46,29] A. Cudd,[6] C. Dalmazzone,[57] T. Daret,[5] Yu. I. Davydov,[39] A. De Roeck,[11] G. De Rosa,[23] T. Dealtry,[34] C. C. Delogu,[24] C. Densham,[58] A. Dergacheva,[26] F. Di Lodovico,[31] S. Dolan,[11] D. Douqa,[12] T. A. Doyle,[43] O. Drapier,[36] J. Dumarchez,[57] P. Dunne,[21] K. Dygnarowicz,[68] A. Eguchi,[59] S. Emery-Schrenk,[5] G. Erofeev,[26] A. Ershova,[5] G. Eurin,[5] D. Fedorova,[26] S. Fedotov,[26] M. Feltre,[24] A. J. Finch,[34] G. A. Fiorentini Aguirre,[74] G. Fiorillo,[23] M. D. Fitton,[58] J. M. Franco Patiño,[54] M. Friend,[15,‡] Y. Fujii,[15,‡] Y. Fukuda,[41] Y. Furui,[63] K. Fusshoeller,[10] L. Giannessi,[12] C. Giganti,[57] V. Glagolev,[39] M. Gonin,[28] J. González Rosa,[54] E. A. G. Goodman,[13] A. Gorin,[26] M. Grassi,[24] M. Guigue,[57] D. R. Hadley,[70] J. T. Haigh,[70] P. Hamacher-Baumann,[53] D. A. Harris,[74] M. Hartz,[66,29] T. Hasegawa,[15,‡] S. Hassani,[5] N. C. Hastings,[15] Y. Hayato,[60,29] D. Henaff,[5] A. Hiramoto,[33] M. Hogan,[7] J. Holeczek,[56] A. Holin,[58] T. Holvey,[46] N. T. Hong Van,[27] T. Honjo,[45] F. Iacob,[24] A. K. Ichikawa,[69] M. Ikeda,[60] T. Ishida,[15,‡] M. Ishitsuka,[64] H. T. Israel,[55] K. Iwamoto,[59] A. Izmaylov,[26] N. Izumi,[64] M. Jakkapu,[15] B. Jamieson,[71] S. J. Jenkins,[37] C. Jesús-Valls,[29] J. J. Jiang,[43] P. Jonsson,[21] S. Joshi,[5] C. K. Jung,[43,§] P. B. Jurj,[21] M. Kabirnezhad,[21] A. C. Kaboth,[52,58] T. Kajita,[61,§] H. Kakuno,[63] J. Kameda,[60] S. P. Kasetti,[38] Y. Kataoka,[60] Y. Katayama,[73] T. Katori,[31] M. Kawaue,[33] E. Kearns,[3,§] M. Khabibullin,[26] A. Khotjantsev,[26] T. Kikawa,[33] H. Kikutani,[59] S. King,[31] V. Kiseeva,[39] J. Kisiel,[56] T. Kobata,[45] H. Kobayashi,[59] T. Kobayashi,[15,‡] L. Koch,[18] S. Kodama,[59] A. Konaka,[66] L. L. Kormos,[34] Y. Koshio,[44,§] A. Kostin,[26] T. Koto,[63] K. Kowalik,[42] Y. Kudenko,[26,∥] Y. Kudo,[73] S. Kuribayashi,[33] R. Kurjata,[68] T. Kutter,[38] M. Kuze,[62] M. La Commara,[23] L. Labarga,[1] K. Lachner,[70] J. Lagoda,[42] S. M. Lakshmi,[42] M. Lamers James,[34,58] M. Lamoureux,[24] A. Langella,[23] J.-F. Laporte,[5] D. Last,[47] N. Latham,[70] M. Laveder,[24] L. Lavitola,[23] M. Lawe,[34] Y. Lee,[33] C. Lin,[21] S.-K. Lin,[38] R. P. Litchfield,[13] S. L. Liu,[43] W. Li,[46] A. Longhin,[24] K. R. Long,[21,58] A. Lopez Moreno,[31] L. Ludovici,[25] X. Lu,[70] T. Lux,[17] L. N. Machado,[13] L. Magaletti,[22] K. Mahn,[40] M. Malek,[55] M. Mandal,[42] S. Manly,[51] A. D. Marino,[6] L. Marti-Magro,[73] D. G. R. Martin,[21] M. Martini,[57,¶] J. F. Martin,[65] T. Maruyama,[15,‡] T. Matsubara,[15] V. Matveev,[26] C. Mauger,[47] K. Mavrokoridis,[37] E. Mazzucato,[5] N. McCauley,[37] J. McElwee,[55] K. S. McFarland,[51] C. McGrew,[43] J. McKean,[21] A. Mefodiev,[26] G. D. Megias,[54] P. Mehta,[37] L. Mellet,[57] C. Metelko,[37] M. Mezzetto,[24] E. Miller,[31] A. Minamino,[73] O. Mineev,[26] S. Mine,[60,4] M. Miura,[60,§] L. Molina Bueno,[19] S. Moriyama,[60,§] S. Moriyama,[73] P. Morrison,[13] Th. A. Mueller,[36] D. Munford,[16] L. Munteanu,[11] K. Nagai,[73] Y. Nagai,[9] T. Nakadaira,[15,‡] K. Nakagiri,[59] M. Nakahata,[60,29] Y. Nakajima,[59] A. Nakamura,[44] H. Nakamura,[64] K. Nakamura,[29,15,‡] K. D. Nakamura,[69] Y. Nakano,[60] S. Nakayama,[60,29] T. Nakaya,[33,29] K. Nakayoshi,[15,‡] C. E. R. Naseby,[21] T. V. Ngoc,[20,**] V. Q. Nguyen,[36] K. Niewczas,[72] S. Nishimori,[15] Y. Nishimura,[30] K. Nishizaki,[45] T. Nosek,[42] F. Nova,[58] P. Novella,[19] J. C. Nugent,[69] H. M. O'Keeffe,[34] L. O'Sullivan,[18] T. Odagawa,[33] T. Ogawa,[15] R. Okada,[44] W. Okinaga,[59] K. Okumura,[61,29] T. Okusawa,[45] N. Ospina,[1] R. A. Owen,[49] Y. Oyama,[15,‡] V. Palladino,[23] V. Paolone,[48] M. Pari,[24] J. Parlone,[37] S. Parsa,[12] J. Pasternak,[21] M. Pavin,[66] D. Payne,[37] G. C. Penn,[37] D. Pershey,[8] L. Pickering,[52] C. Pidcott,[55] G. Pintaudi,[73] C. Pistillo,[2] B. Popov,[57,††] K. Porwit,[56] M. Posiadala-Zezula,[67] Y. S. Prabhu,[42] F. Pupilli,[24] B. Quilain,[36] T. Radermacher,[53] E. Radicioni,[22] B. Radics,[74] M. A. Ramírez,[47] P. N. Ratoff,[34] M. Reh,[6] C. Riccio,[43] E. Rondio,[42] S. Roth,[53] N. Roy,[74] A. Rubbia,[10] A. C. Ruggeri,[23] C. A. Ruggles,[13] A. Rychter,[68] K. Sakashita,[15,‡] F. Sánchez,[12] G. Santucci,[74] C. M. Schloesser,[12] K. Scholberg,[8,§] M. Scott,[21] Y. Seiya,[45,‡‡] T. Sekiguchi,[15,‡] H. Sekiya,[60,29,§] D. Sgalaberna,[10] A. Shaikhiev,[26] F. Shaker,[74] M. Shiozawa,[60,29] W. Shorrock,[21] A. Shvartsman,[26] N. Skrobova,[26] K. Skwarczynski,[42] D. Smyczek,[53] M. Smy,[4] J. T. Sobczyk,[72] H. Sobel,[4,29] F. J. P. Soler,[13] Y. Sonoda,[60] A. J. Speers,[34] R. Spina,[22] I. A. Suslov,[39] S. Suvorov,[26,57] A. Suzuki,[32] S. Y. Suzuki,[15,‡] Y. Suzuki,[29] A. A. Sztuc,[21] M. Tada,[15,‡] S. Tairafune,[69] S. Takayasu,[45] A. Takeda,[60] Y. Takeuchi,[32,29] K. Takifuji,[69] H. K. Tanaka,[60,§] Y. Tanihara,[73] M. Tani,[33] A. Teklu,[43] V. V. Tereshchenko,[39] N. Teshima,[45] N. Thamm,[53] L. F. Thompson,[55] W. Toki,[7] C. Touramanis,[37] T. Towstego,[65] K. M. Tsui,[37] T. Tsukamoto,[15,‡] M. Tzanov,[38] Y. Uchida,[21] M. Vagins,[29,4] D. Vargas,[17] M. Varghese,[17] G. Vasseur,[5] C. Vilela,[11] E. Villa,[11,12] W. G. S. Vinning,[70] U. Virginet,[57] T. Vladisavljevic,[58] T. Wachala,[14] J. G. Walsh,[40] Y. Wang,[43] L. Wan,[3] D. Wark,[58,46] M. O. Wascko,[21] A. Weber,[18] R. Wendell,[33,§] M. J. Wilking,[43] C. Wilkinson,[35] J. R. Wilson,[31] K. Wood,[35] C. Wret,[46] J. Xia,[29] Y.-h. Xu,[34] K. Yamamoto,[45,‡‡]

T. Yamamoto,[45] C. Yanagisawa,[43,§§] G. Yang,[43] T. Yano,[60] K. Yasutome,[33] N. Yershov,[26] U. Yevarouskaya,[57] M. Yokoyama,[59,§] Y. Yoshimoto,[59] N. Yoshimura,[33] M. Yu,[74] R. Zaki,[74] A. Zalewska,[14] J. Zalipska,[42] K. Zaremba,[68] G. Zarnecki,[14] X. Zhao,[10] T. Zhu,[21] M. Ziembicki,[68] E. D. Zimmerman,[6] M. Zito,[57] and S. Zsoldos[31]

(T2K Collaboration)

[1]*University Autonoma Madrid, Department of Theoretical Physics, 28049 Madrid, Spain*
[2]*University of Bern, Albert Einstein Center for Fundamental Physics, Laboratory for High Energy Physics (LHEP), Bern, Switzerland*
[3]*Boston University, Department of Physics, Boston, Massachusetts, USA*
[4]*University of California, Irvine, Department of Physics and Astronomy, Irvine, California, USA*
[5]*IRFU, CEA, Université Paris-Saclay, F-91191 Gif-sur-Yvette, France*
[6]*University of Colorado at Boulder, Department of Physics, Boulder, Colorado, USA*
[7]*Colorado State University, Department of Physics, Fort Collins, Colorado, USA*
[8]*Duke University, Department of Physics, Durham, North Carolina, USA*
[9]*Eötvös Loránd University, Department of Atomic Physics, Budapest, Hungary*
[10]*ETH Zurich, Institute for Particle Physics and Astrophysics, Zurich, Switzerland*
[11]*CERN European Organization for Nuclear Research, CH-1211 Genéve 23, Switzerland*
[12]*University of Geneva, Section de Physique, DPNC, Geneva, Switzerland*
[13]*University of Glasgow, School of Physics and Astronomy, Glasgow, United Kingdom*
[14]*H. Niewodniczanski Institute of Nuclear Physics PAN, Krakow, Poland*
[15]*High Energy Accelerator Research Organization (KEK), Tsukuba, Ibaraki, Japan*
[16]*University of Houston, Department of Physics, Houston, Texas, USA*
[17]*Institut de Fisica d'Altes Energies (IFAE)—The Barcelona Institute of Science and Technology, Campus UAB, Bellaterra (Barcelona) Spain*
[18]*Institut für Physik, Johannes Gutenberg-Universität Mainz, Staudingerweg 7, 55128 Mainz, Germany*
[19]*IFIC (CSIC and University of Valencia), Valencia, Spain*
[20]*Institute For Interdisciplinary Research in Science and Education (IFIRSE), ICISE, Quy Nhon, Vietnam*
[21]*Imperial College London, Department of Physics, London, United Kingdom*
[22]*INFN Sezione di Bari and Università e Politecnico di Bari, Dipartimento Interuniversitario di Fisica, Bari, Italy*
[23]*INFN Sezione di Napoli and Università di Napoli, Dipartimento di Fisica, Napoli, Italy*
[24]*INFN Sezione di Padova and Università di Padova, Dipartimento di Fisica, Padova, Italy*
[25]*INFN Sezione di Roma and Università di Roma "La Sapienza," Roma, Italy*
[26]*Institute for Nuclear Research of the Russian Academy of Sciences, Moscow, Russia*
[27]*International Centre of Physics, Institute of Physics (IOP), Vietnam Academy of Science and Technology (VAST), 10 Dao Tan, Ba Dinh, Hanoi, Vietnam*
[28]*ILANCE, CNRS—University of Tokyo International Research Laboratory, Kashiwa, Chiba 277-8582, Japan*
[29]*Kavli Institute for the Physics and Mathematics of the Universe (WPI), The University of Tokyo Institutes for Advanced Study, University of Tokyo, Kashiwa, Chiba, Japan*
[30]*Keio University, Department of Physics, Kanagawa, Japan*
[31]*King's College London, Department of Physics, Strand, London WC2R 2LS, United Kingdom*
[32]*Kobe University, Kobe, Japan*
[33]*Kyoto University, Department of Physics, Kyoto, Japan*
[34]*Lancaster University, Physics Department, Lancaster, United Kingdom*
[35]*Lawrence Berkeley National Laboratory, Berkeley, California 94720, USA*
[36]*Ecole Polytechnique, IN2P3-CNRS, Laboratoire Leprince-Ringuet, Palaiseau, France*
[37]*University of Liverpool, Department of Physics, Liverpool, United Kingdom*
[38]*Louisiana State University, Department of Physics and Astronomy, Baton Rouge, Louisiana, USA*
[39]*Joint Institute for Nuclear Research, Dubna, Moscow Region, Russia*
[40]*Michigan State University, Department of Physics and Astronomy, East Lansing, Michigan, USA*
[41]*Miyagi University of Education, Department of Physics, Sendai, Japan*
[42]*National Centre for Nuclear Research, Warsaw, Poland*
[43]*State University of New York at Stony Brook, Department of Physics and Astronomy, Stony Brook, New York, USA*
[44]*Okayama University, Department of Physics, Okayama, Japan*
[45]*Osaka Metropolitan University, Department of Physics, Osaka, Japan*
[46]*Oxford University, Department of Physics, Oxford, United Kingdom*

[47]*University of Pennsylvania, Department of Physics and Astronomy, Philadelphia, Pennsylvania 19104, USA*
[48]*University of Pittsburgh, Department of Physics and Astronomy, Pittsburgh, Pennsylvania, USA*
[49]*Queen Mary University of London, School of Physics and Astronomy, London, United Kingdom*
[50]*University of Regina, Department of Physics, Regina, Saskatchewan, Canada*
[51]*University of Rochester, Department of Physics and Astronomy, Rochester, New York, USA*
[52]*Royal Holloway University of London, Department of Physics, Egham, Surrey, United Kingdom*
[53]*RWTH Aachen University, III. Physikalisches Institut, Aachen, Germany*
[54]*Departamento de Física Atómica, Molecular y Nuclear, Universidad de Sevilla, 41080 Sevilla, Spain*
[55]*University of Sheffield, Department of Physics and Astronomy, Sheffield, United Kingdom*
[56]*University of Silesia, Institute of Physics, Katowice, Poland*
[57]*Sorbonne Université, Université Paris Diderot, CNRS/IN2P3, Laboratoire de Physique Nucléaire et de Hautes Energies (LPNHE), Paris, France*
[58]*STFC, Rutherford Appleton Laboratory, Harwell Oxford and Daresbury Laboratory, Warrington, United Kingdom*
[59]*University of Tokyo, Department of Physics, Tokyo, Japan*
[60]*University of Tokyo, Institute for Cosmic Ray Research, Kamioka Observatory, Kamioka, Japan*
[61]*University of Tokyo, Institute for Cosmic Ray Research, Research Center for Cosmic Neutrinos, Kashiwa, Japan*
[62]*Tokyo Institute of Technology, Department of Physics, Tokyo, Japan*
[63]*Tokyo Metropolitan University, Department of Physics, Tokyo, Japan*
[64]*Tokyo University of Science, Faculty of Science and Technology, Department of Physics, Noda, Chiba, Japan*
[65]*University of Toronto, Department of Physics, Toronto, Ontario, Canada*
[66]*TRIUMF, Vancouver, British Columbia, Canada*
[67]*University of Warsaw, Faculty of Physics, Warsaw, Poland*
[68]*Warsaw University of Technology, Institute of Radioelectronics and Multimedia Technology, Warsaw, Poland*
[69]*Tohoku University, Faculty of Science, Department of Physics, Miyagi, Japan*
[70]*University of Warwick, Department of Physics, Coventry, United Kingdom*
[71]*University of Winnipeg, Department of Physics, Winnipeg, Manitoba, Canada*
[72]*Wroclaw University, Faculty of Physics and Astronomy, Wroclaw, Poland*
[73]*Yokohama National University, Department of Physics, Yokohama, Japan*
[74]*York University, Department of Physics and Astronomy, Toronto, Ontario, Canada*

(Received 19 May 2023; accepted 15 September 2023; published 12 October 2023)

Muon neutrino and antineutrino disappearance probabilities are identical in the standard three-flavor neutrino oscillation framework, but *CPT* violation and nonstandard interactions can violate this symmetry. In this work we report the measurements of $\sin^2\theta_{23}$ and Δm^2_{32} independently for neutrinos and antineutrinos. The aforementioned symmetry violation would manifest as an inconsistency in the neutrino and antineutrino oscillation parameters. The analysis discussed here uses a total of 1.97×10^{21} and 1.63×10^{21} protons on target taken with a neutrino and antineutrino beam respectively, and benefits from improved flux and cross section models, new near-detector samples and more than double the data reducing

[*]Also at Université Paris-Saclay.
[†]Also at INFN-Laboratori Nazionali di Legnaro.
[‡]Also at J-PARC, Tokai, Japan.
[§]Also an affiliated member at Kavli IPMU (WPI), the University of Tokyo, Japan.
[‖]Also at Moscow Institute of Physics and Technology (MIPT), Moscow region, Russia and National Research Nuclear University "MEPhI," Moscow, Russia.
[¶]Also at IPSA-DRII, France.
[**]Also at the Graduate University of Science and Technology, Vietnam Academy of Science and Technology.
[††]Also at JINR, Dubna, Russia.
[‡‡]Also at Nambu Yoichiro Institute of Theoretical and Experimental Physics (NITEP).
[§§]Also at BMCC/CUNY, Science Department, New York, New York, USA.

the overall uncertainty of the result. No significant deviation is observed, consistent with the standard neutrino oscillation picture.

DOI: 10.1103/PhysRevD.108.072011

I. INTRODUCTION

Neutrino oscillations are described by the Pontecorvo-Maki-Nakagawa-Sakata (PMNS) matrix, U_{lj}, which relates the neutrino mass eigenstates ν_j [with masses $m_j = (m_1, m_2, m_3)$] to the left-handed neutrino flavor fields ν_l (ν_e, ν_μ, ν_τ) [1,2] as $\nu_l = \sum_j U_{lj}\nu_j$. The matrix U_{lj} is parametrized by three mixing angles θ_{12}, θ_{13}, and θ_{23}, and a CP-violating phase δ_{CP}. Two Majorana phases appear on the diagonal terms in U_{lj} if the neutrino is the same as its antiparticle, but they have no effect on neutrino oscillations. In this framework, ν_μ and $\bar{\nu}_\mu$ disappearance probabilities are the same in the absence of matter effects (which are negligible at T2K energies and baseline, but are included in their calculation) so a mismatch could indicate a source of CPT violation (since CPT $[P(\nu_\mu \to \nu_\mu)] = P(\bar{\nu}_\mu \to \bar{\nu}_\mu)$ in vacuum) or a source of nonstandard interactions [3].

The results presented in this paper represent an update to the previous T2K measurements [4–6]. Like these previous analyses, we allow the oscillation parameters for ν_μ (θ_{23}, Δm^2_{32}) to vary separately from those of $\bar{\nu}_\mu$ ($\bar{\theta}_{23}$, $\Delta\bar{m}^2_{32}$), while all other oscillation parameters are assumed to be the same for neutrinos and antineutrinos.

This work is organized as follows. First, an overview of the T2K experimental setup is given in Sec. II. The analysis method is then described in Sec. III. Finally, the results are discussed in Sec. IV and conclusions are presented in Sec. V.

II. T2K EXPERIMENTAL SETUP

T2K is a long-baseline neutrino oscillation experiment located in Japan [7]. A neutrino beam produced at the Japan Proton Accelerator Research Complex (J-PARC) is directed towards Super-Kamiokande (SK) [8,9], a large water Cherenkov detector.

The neutrino beam is produced by 30 GeV protons impinging on a graphite target. Interactions in the target produce hadrons, which are focused using three magnetic horns [10]. The polarity of the magnetic field produced by the horns is reversible, allowing for the selection of positively (negatively) charged hadrons which then decay into a beam dominated by muon neutrinos (antineutrinos).

A suite of near detectors is situated 280 m downstream of the beam production target. The stability and direction of the neutrino beam are monitored using the on-axis near detector INGRID [11]. INGRID consists of 14 detector modules arranged in a cross formation, with each module containing sandwiched layers of iron plates and scintillator planes [12]. A second near detector, ND280, is positioned 2.5° off-axis from the neutrino beamline. It is used to measure the unoscillated neutrino flux and neutrino interaction parameters in order to constrain systematic errors in the oscillation analysis. ND280 consists of a π^0 detector [13] followed by three time-projection chambers (TPCs) [14] interleaved with two fine-grained detectors (FGDs) [15], all surrounded by an electromagnetic calorimeter [16]. ND280 is also magnetized to allow for the charge identification of particles. The gaps in the magnet yoke are instrumented by muon range detectors [17].

SK is a 50 kt water Cherenkov detector situated 295 km downstream of the neutrino production point and is positioned at the same off-axis angle as ND280. In this configuration, the beam has a peak energy around 0.6 GeV that maximizes the effect of neutrino oscillations. It has optically separated inner detector (ID) and outer detector (OD) volumes. It uses 11,129 inward-facing 20-inch photomultiplier tubes (PMTs) to detect Cherenkov radiation from charged particles traversing the detector. To reject interactions from outside the ID volume, 1885 outward-facing 8-inch PMTs in the OD are used. SK is able to discriminate between electrons and muons by their Cherenkov ring profiles [18].

III. ANALYSIS METHOD

The analysis strategy presented here is similar to the one employed in previous analyses [4–6]. First, we define a model that predicts the event spectra at both the near and far detectors. Such predictions are extracted by simulating the neutrino flux and cross sections, tuned to external experimental data, and the detector response. This model is then fit to the ND280 data to obtain tuned values and constraints for the flux systematic uncertainties and a subset of the cross section systematic uncertainties. The results of the near-detector analysis are propagated to SK as a multivariate normal distribution described by a covariance matrix and the best-fit values for each parameter associated to neutrino flux and cross section systematic uncertainties. At this point, we perform a fit to SK data to extract the oscillation parameters. Four significant updates have been made since the previous analysis. First, the number of protons on target (POT) collected in neutrino beam mode was increased from 1.49×10^{21} to 1.97×10^{21} by including T2K data up to February 2020. Second, the flux prediction was tuned to the $\pi^{\pm}$ yields from the surface of a T2K replica target measured by NA61/SHINE [19]. Third, the modeling of neutrino interactions on nuclear targets was improved.

Finally, the selection of antineutrino events at ND280 was refined and the data set doubled.

A. Flux prediction

The neutrino flux prediction used for this analysis has been upgraded from a tuning [20,21] based on thin target measurements [22] to a tuning of charged pion yields [19] measured by NA61/SHINE using a replica of the T2K target. The details of the new tuning are described in Ref. [23], which is also summarized below.

Incoming protons are generated according to beam profiles measured for each run, and their hadronic interactions inside the 90 cm long graphite target are simulated with FLUKA version 2011.2x [24,25]. The particles emitted from the target are then focused by the three magnetic horns and tracked until they decay into neutrinos in the decay volume using the GEANT3-based Jnubeam package [21]. Charged pions exiting from the target are tuned using tuning factors based on replica target measurements, which depend on the exiting longitudinal position, momentum, and direction with respect to the target axis. For exiting particles not covered by the replica target measurements, such as kaons and protons and any hadronic interactions outside of the target, cross section, and multiplicity tuning based on thin target measurements is applied to each interaction as in previous analyses. The statistical and systematic uncertainties on the NA61/SHINE measured yields are then propagated to the flux to estimate the uncertainty on the hadron interactions. For interactions unconstrained by external data, uncertainties are assigned based on comparisons between Monte Carlo (MC) hadron interaction models. Together with other uncertainties on proton beam profile parameters and beamline alignment, a covariance matrix of the flux at the near and far detectors for each neutrino flavor in the two beam modes is constructed. This is then used to propagate the neutrino flux constraint at the near detector to the far detector prediction.

The new tuning, extrapolated using the NA61/SHINE 2009 replica target data, reduces the relative uncertainty of the ν_μ flux in ν-mode and $\bar{\nu}_\mu$ flux in $\bar{\nu}$ -mode from about 9–12% to 5–8% near the flux peak. For the $\bar{\nu}_\mu$ component in ν-mode and ν_μ component in $\bar{\nu}$ -mode (the so-called “wrong-sign background”), the uncertainty has a larger contribution from interactions occurring outside the main target, resulting in a relative uncertainty of about 6–8%.

B. Neutrino interaction modeling

Neutrino and antineutrino interactions are simulated using the MC event generator NEUT version 5.4.0 [26]. The main interaction channels in the range of energies relevant for T2K are: charged-current quasielastic scattering (CCQE), 2p2h (“two particle, two hole”) interactions, resonant pion production (RES), and deep inelastic scattering (DIS). 2p2h interactions occur when neutrinos interact with correlated pairs of nucleons, ejecting both from the nucleus. Furthermore, hadrons produced in neutrino interactions on nuclei can interact with the nuclear medium, undergoing so-called final state interactions (FSI). CCQE interactions are simulated according to the Llewellyn-Smith formalism [27] with a dipole axial form factor and BBBA05 vector form factors [28]. In this analysis, we moved from the relativistic Fermi gas (RFG) nuclear model to the spectral function (SF) model described in Ref. [29], with an axial mass $M_A^{\mathrm{QE}} = 1.03$ GeV tuned to bubble chamber data [30,31]. The 2p2h interactions are simulated according to the Valencia model described in Ref. [32]. The model for RES is based on the Rein-Sehgal model [33] for events with an invariant hadronic mass $W \leq 2$ GeV (natural units are used throughout the paper), with updated nucleon form factors [34]. The DIS interaction is calculated for events with invariant hadronic mass $W > 1.3$ GeV, using GRV98 parton distribution functions [35] with Bodek-Yang corrections [36]. For $1.3\ \mathrm{GeV} < W < 2\ \mathrm{GeV}$, only DIS interactions that produce more than one pion are simulated to avoid double counting with the nonresonant single pion production. For values of $W \leq 2$ GeV a custom hadronization [37] is employed, whilst for $W > 2$ GeV PYTHIA/JetSet [38] is used. Pion FSIs are simulated using a semi-classical intranuclear cascade model by Salcedo and Oset [39,40], tuned to recent $\pi^\pm$-nucleus scattering data [41]. Nucleon FSIs are described in an analogous cascade model [26]. The Coulomb interaction between the outgoing charged lepton and the nucleus is implemented as a nucleus- and lepton- flavor-dependent shift in the momentum of the outgoing lepton. The size of such a shift has been determined from an analysis of electron scattering data to be $\sim \pm 5$ MeV/c [42]. Every parameter relevant to the particular channel described above has uncertainties associated to it. The parametrization employed and such uncertainties are often driven by theory, but additional empirically driven parameters are used since the first alone cannot describe the available neutrino cross section data. Important changes compared to the previous analysis are a new treatment of the removal energy for CCQE interactions, the freedom to change the CCQE cross section normalization as a function of the momentum transferred, and improved FSIs uncertainties.

Contrary to the Fermi-gas models, the SF model does not have a fixed value for the nuclear binding energy and it can be varied as a parameter. The removal energy shifts are encoded in four parameters depending on whether they affect initial-state protons or neutrons, and if the target is carbon or oxygen. These parameters shift the outgoing lepton momentum of a CCQE interaction and depend on the lepton kinematics, neutrino energy, and flavor.

Recent measurements of the charged-current interactions without mesons in the final state performed by

MINERνA [43,44] and T2K [45,46] show a clear suppression at low-Q^2. In previous T2K analyses that used the Fermi-gas model [23] this suppression is achieved by including a nuclear screening effect using the random phase approximation (RPA) [47]. Since the SF model employed in this analysis does not include this suppression, five unconstrained parameters that alter the normalization of the CCQE cross section in the range $Q^2 = \{0, 0.25\}$ GeV^2 were included. This range is split into subranges of 0.05 GeV^2. For values of the momentum transferred larger than 0.25 GeV^2 three parameters are used to account for deviation from the dipole model.

Finally, the NEUT pion cascade model has been tuned to external $\pi - A$ scattering data [48].

C. Near-detector analysis

The near detector complex is used to measure the properties of the neutrino beam before it oscillates. These measurements allow for a reduction of the systematic uncertainties that affect event rates at SK.

An extended likelihood fit as a function of the reconstructed muon momentum and outgoing angle measured at ND280 is performed to constrain the (anti)neutrino flux and cross section modeling. Prior constraints are included as penalty terms. A total of 18 samples of ν_μ and $\bar{\nu}_\mu$ charged-current (CC) interactions with vertices in either of the FGDs are employed in this fit. Their selection is optimized to maximize the sensitivity of ND280 to different features of the (anti)neutrino spectra. Event selections are based on the requirement that the highest-momentum track is compatible with the muon hypothesis according to the TPC particle identification. This track is required to be negatively charged if the selection is performed in ν-mode, but either positively or negatively charged in $\bar{\nu}$ -mode to also identify the relatively large ν_μ background component of the $\bar{\nu}$ -mode. As in the previous analysis [4], in ν-mode the sample of ν_μ CC interactions is further split into three subsamples according to the pion multiplicity in the final state; CC events without reconstructed pions (CC-0π), with one reconstructed positively-charged pion (CC-1π^+), and all remaining CC events (CC-Other). In $\bar{\nu}$ -mode, thanks to the increased statistics, we moved from a selection based on the track multiplicity to one that matches the selection adopted in ν-mode. Such improvement was possible for both $\bar{\nu}_\mu$ and ν_μ background components, resulting in six $\bar{\nu}$ -mode samples for each FGD. The main difference is related to the selection of $\bar{\nu}_\mu$ CC events with one reconstructed negatively-charged pion. They are identified by employing the particle identification capabilities of the TPC and FGD, and tagging the Michel electron produced in the $\pi \to \mu \to e$ decay chain. Since negatively-charged pions are more likely to be absorbed in the material of the FGD, if a Michel electron is tagged, the associated pion in 63% of the cases is positively charged. The detector response is evaluated using dedicated control samples as detailed in Ref. [49]. Compared with previous analyses, pion secondary interactions (SI) are simulated using the semi-classical cascade model in NEUT, in place of the model used in previous analyses from GEANT4. The model was tuned to $\pi^\pm$-nucleus scattering data mentioned previously, which improved the agreement with data, reducing the systematic error associated with pion SI.

Once the likelihood fit is performed, we calculate the p-value to quantify the ability of the best-fit point to describe the data, i.e. the probability of observing an outcome as or more extreme than data according to the model. It is computed as the fraction of fits for which the computed χ^2 when varying the model is greater than the one computed for the fit to the data. We define p-values below 5% as indicating a significant disagreement with the model. Over 895 variations of our model, we find a p-value of 74%, much larger than this threshold. The result of the near-detector analysis is parametrized as a multivariate Gaussian constraint in the analysis employed to extract the oscillation parameters (θ_{23}, Δm^2_{32}) and ($\bar{\theta}_{23}$, $\Delta \bar{m}^2_{32}$).

D. Far-detector event selection

This analysis uses two muonlike event samples at the far detector; one with the beam in ν-mode and one with the beam in $\bar{\nu}$ -mode. This allows for the oscillations of ν_μ and $\bar{\nu}_\mu$ to be measured separately despite the inability of SK to distinguish negatively charged and positively charged muons. The wrong-sign background in $\bar{\nu}$ -mode is constrained by the ν-mode samples by performing a combined analysis of the ν- and $\bar{\nu}$ -mode samples.

Charge and timing information from the SK PMTs are used to reconstruct the vertex position, momentum, and particle identification (PID) of events inside the detector. Particles are identified by their Cherenkov ring profiles. Due to their larger mass, muons are more resilient to scattering, resulting in clear rings with well-defined edges. In contrast, electrons scatter more and produce electromagnetic showers, resulting in rings with diffuse edges. The reconstruction algorithm [18] also counts Michel electrons by identifying delayed hit timing clusters.

The samples used in this analysis, referred to as 1Rμ, select for reconstructed events with one muonlike ring and no other rings, and 0 or 1 delayed Michel electrons. The number of predicted (postnear-detector analysis) and observed events for both 1Rμ samples are shown in Table I. Note that the number of $\bar{\nu}$ -mode 1Rμ data events differs from the previous analysis described in Ref. [4] due to updated data processing at SK, as described in Ref. [23]. The increased exposure reduced the statistical uncertainty on the number of ν-mode 1Rμ events by 13%, resulting in 5.6%.

TABLE I. Number of predicted events and data events selected for both 1Rμ samples. The predictions are calculated assuming $\Delta m^2_{21} = 7.53 \times 10^{-5}$ eV^2, $\Delta m^2_{32} = 2.509 \times 10^{-3}$ eV^2, $\sin^2\theta_{23} = 0.528$, $\sin^2\theta_{12} = 0.307$, $\sin^2\theta_{13} = 0.0218$, $\delta_{CP} = -1.601$, Earth matter density of 2.6 g cm^{-3}, and normal mass ordering.

Sample	Prediction	Data
ν-mode 1Rμ	345.3	318
$\bar{\nu}$ -mode 1Rμ	135.2	137

E. Impact of systematic uncertainties

The systematic uncertainties we include in this analysis are associated with neutrino beam flux modeling, neutrino interaction cross section modeling, and detector response. The first two sources of systematic uncertainties are constrained by fitting our model to the ND280 near-detector data as described in Sec. III C. The systematic uncertainties constrained by the near detector are included as input constraints in the far-detector analysis. Table II shows the contribution to the total relative uncertainty from each source of the systematic error on the predicted number of events in each SK sample. Both ν- and $\bar{\nu}$ -mode are reduced from 12% to 3% and 4%, respectively thanks to the near-detector analysis. Some cross section systematics are not constrained by the near detector. The larger relative error on the 1Rμ $\bar{\nu}$ sample is mainly due to the large uncertainty in low-energy pion-production modeling. The far detector systematic error (SK det.) includes uncertainties in ring counting efficiencies, event selection, fiducial volume, secondary particle interactions, and photonuclear effects.

Compared with the previous analysis, the total systematic error was reduced by 45% and 9%, for the 1Rμ ν-mode and $\bar{\nu}$-mode event rates respectively. As expected, this improvement is driven by the new flux tuning and new neutrino interaction modeling that are reduced overall by 36% and 21% for the two samples. The total systematic error must be compared with the statistical uncertainty which is 5.6% and 8.5%.

TABLE II. Uncertainties on the number of events in each SK sample broken down by error source after the near-detector analysis. The first two rows show the uncertainties when flux and cross section systematics (constrained by the near detector) are propagated without correlation, whereas the third (Flux + Xsec) has smaller uncertainties due to the anticorrelations in the near-detector analysis, and corresponds to what is used in the analysis. "SK det." includes uncertainties from the SK detector response.

Error source (units: %)	1Rμ ν-mode	1Rμ $\bar{\nu}$-mode
Flux	2.9	2.8
Xsec (ND constrained)	3.1	3.0
Flux + Xsec (ND constrained)	2.1	2.3
SK-only Xsec	0.6	2.5
SK detector	2.1	1.9
Total	3.0	4.0

F. Oscillation analysis

The oscillation probabilities are calculated using a slight modification of the 3-flavor PMNS oscillation framework. The ν_μ survival probability, not including the matter effect for simplicity, is approximately given by

$$P(\overset{(-)}{\nu}_\mu \to \overset{(-)}{\nu}_\mu) \simeq 1 - (\cos^4\theta_{13}\sin^2 2\overset{(-)}{\theta}_{23} + \sin^2 2\theta_{13}\sin^2\overset{(-)}{\theta}_{23}) \times \sin^2\left(\frac{\Delta \overset{(-)}{m}{}^2_{32} L}{4E}\right) \tag{1}$$

where the barred parameters correspond to muon antineutrino oscillations. The standard PMNS formalism is recovered when $(\sin^2\theta_{23}, \Delta m^2_{32}) = (\sin^2\bar{\theta}_{23}, \Delta\bar{m}^2_{32})$. Note that the full ν_μ survival probability is employed in the analysis. In the oscillation analysis, neutrino and antineutrino parameters are varied independently and fitted simultaneously to data by minimizing the combined negative log-likelihood $-\ln\mathcal{L} = \sum_i (N_i^{\mathrm{exp}} - N_i^{\mathrm{obs}} + N_i^{\mathrm{obs}} \times \ln(N_i^{\mathrm{obs}}/N_i^{\mathrm{exp}}))$ calculated for both muon neutrino and muon antineutrino samples binned in reconstructed neutrino energy and muon scattering angle, where N_i^{exp} is the number of predicted events in the ith bin and N_i^{obs} is the number of observed events. All systematic uncertainties and other oscillation parameters, such as $\sin^2 2\theta_{13}$ and δ_{CP}, are treated as nuisance parameters and are marginalized over according to their assigned priors. This marginal likelihood is used to construct confidence intervals using the fixed $\Delta\chi^2$ method [50]. Since the μ-like samples are not sensitive to neutrino mass ordering or $\sin^2 2\theta_{13}$, we assume normal ordering in this analysis and constrain $\sin^2 2\theta_{13}$ by the Ref. [51] value from reactor experiments. As the survival probability from Eq. (1) is symmetric in the sign of $\pm(\cos^2\theta_{13}\sin^2\overset{(-)}{\theta}_{23} - 1/2)$, the constraints on $\sin^2\overset{(-)}{\theta}_{23}$ will be symmetric about $0.5/\cos^2\theta_{13} \approx 0.511$; in the standard PMNS formalism analysis this symmetry is broken by the inclusion of ν_e and $\bar{\nu}_e$ samples. A flat prior is used for δ_{CP}. The robustness of the analysis is assessed by repeated tests using a variety of simulated data sets with alternative interaction models. The bias on the parameters of interest is estimated as well.

IV. RESULTS AND DISCUSSION

The reconstructed energy distributions for ν-mode and $\bar{\nu}$ -mode 1Rμ samples for data taken from January 2010 to February 2020 (run 1–10) and the best-fit predictions are shown in Fig. 1. The results of the three-flavor analysis using both electronlike and muonlike samples as described in Ref. [23] are also shown for comparison. In both cases, the prediction and data agree within the statistical uncertainties indicated by the error bars.

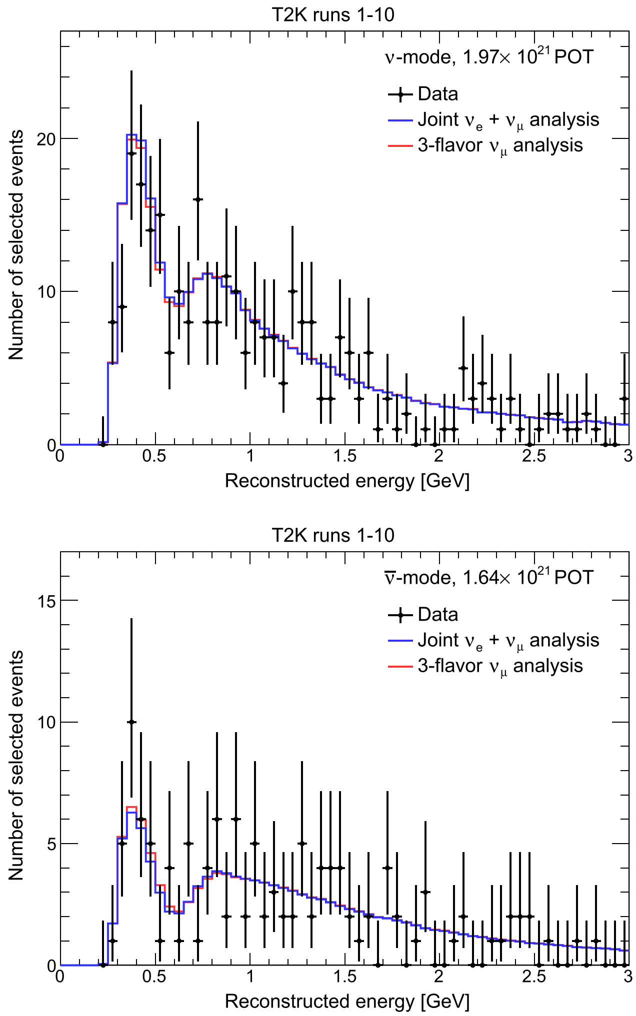

FIG. 1. The reconstructed neutrino energy distributions for neutrino (top) and antineutrino (bottom) mode 1Rμ samples. The lines show the predicted number of events under two hypotheses: "Joint $\nu_e + \nu_\mu$ analysis" uses the best-fit values from a joint analysis of the PMNS model to electronlike and muonlike samples [23], "3-flavor ν_μ analysis" (this analysis) uses the best-fit from the analysis reported here. The error bars indicate the statistical uncertainties.

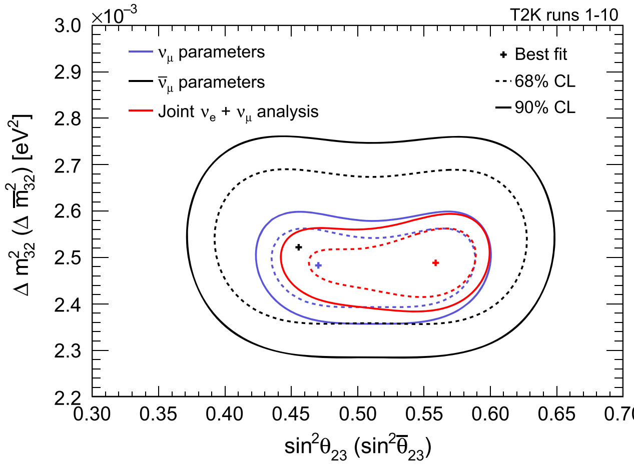

FIG. 2. Confidence regions of $(\sin^2\theta_{23}, \Delta m^2_{32})$ for neutrinos and their barred parameters for antineutrinos. Corresponding regions from the standard PMNS formalism analysis [23] including ν_e samples are also shown for comparison.

The best-fit values obtained for oscillation parameters describing neutrino oscillations are $\sin^2\theta_{23} = 0.47^{+0.11}_{-0.02}$ and $\Delta m^2_{32} = 2.48^{+0.05}_{-0.06} \times 10^{-3}\ \mathrm{eV}^2$ and those describing antineutrino oscillations are $\sin^2\bar{\theta}_{23} = 0.45^{+0.16}_{-0.04}$ and $\Delta\bar{m}^2_{32} = 2.53^{+0.10}_{-0.11} \times 10^{-3}\ \mathrm{eV}^2$. The best-fit values for both neutrino and antineutrino oscillations agree within the uncertainties.

Based on the robustness checks, the bias on Δm^2_{32} introduced by the limited flexibility of the neutrino interactions model for ν-mode ($\bar{\nu}$ -mode) is estimated to be $1.40\,(1.55) \times 10^{-5}\ \mathrm{eV}^2$, which is accounted for in the analysis by smearing the $\Delta\chi^2$ contour with additional Gaussian uncertainty. As for the analysis in Ref. [23], the biggest bias was observed using an alternative model for pion secondary interactions. No bias is observed on the other oscillation parameters.

In Fig. 2 we compare the constraints on $\sin^2 \overset{(-)}{\theta}_{23}$ and $\Delta \overset{(-)}{m}{}^2_{32}$ coming from the three-flavor analysis to muonlike samples and the joint analysis to both electronlike and muonlike samples [23]. Since the parameters for ν_μ and $\bar{\nu}_\mu$ are compatible, this analysis does not provide indication of new physics. The ν_μ-only analysis results are not sensitive to the θ_{23} octant due to the lack of electronlike samples in the analysis.

Figure 3 shows a comparison to the results obtained in the previous analysis and an intermediate step to show the contribution of the updated analysis model. The analysis

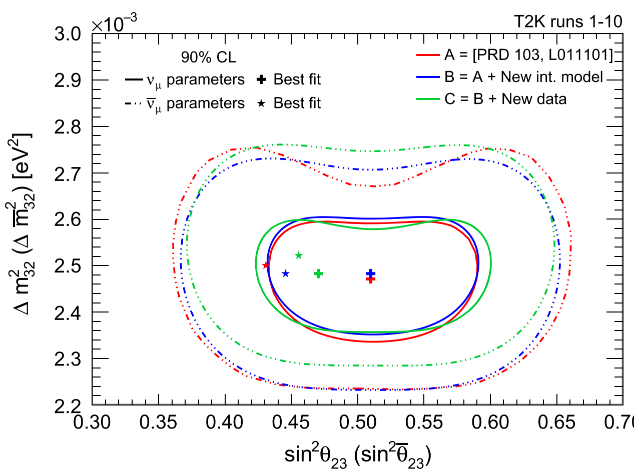

FIG. 3. Comparison of the 90% confidence level in $(\sin^2\theta_{23}, \Delta m^2_{32})$ and their barred counterparts for antineutrinos (dot-dashed lines) to those obtained in the previous analysis (red line), an intermediate step showing the contribution of the updated analysis model (blue line), and the final results of this analysis including new SK neutrino mode data and updated data processing (green line).

model is found to change the shape of the antineutrino parameter contours, whereas the new data at SK improve the background constraint and move the neutrino parameters away from maximal mixing. The new SK data also move the antineutrino parameters to slightly larger values, but compatible, of $\Delta\bar{m}^2_{32}$ and $\sin^2\bar{\theta}_{23}$, which is also affected by the updated data processing.

V. CONCLUSIONS

We have presented the results from the muon (anti) neutrino oscillation analysis to T2K data corresponding to a total of 3.6×10^{21} POT taken in neutrino and antineutrino mode. The predictions for each SK sample are based on the constraints provided by the near-detector analysis. We conclude that the measurements of the parameters describing the oscillations of muon neutrinos and antineutrinos are compatible with the three-flavor prediction and provide no indication of new physics.

The data related to this work can be found in Ref. [52].

ACKNOWLEDGMENTS

We thank the J-PARC staff for superb accelerator performance. We thank the CERN NA61/SHINE Collaboration for providing valuable particle production data. We acknowledge the support of MEXT, JSPS KAKENHI (JP16H06288, JP18K03682, JP18H03701, JP18H05537, JP19J01119, JP19J22440, JP19J22258, JP20H00162, JP20H00149, JP20J20304) and bilateral programs (JPJSBP120204806, JPJSBP120209601), Japan; NSERC, the NRC, and CFI, Canada; the CEA and CNRS/IN2P3, France; the DFG (RO 3625/2), Germany; the INFN, Italy; the Ministry of Education and Science (2023/WK/04) and the National Science Centre (UMO-2018/30/E/ST2/00441 and UMO-2022/46/E/ST2/00336), Poland; the RSF19-12-00325, RSF22-12-00358, Russia; MICINN (SEV-2016-0588, PID2019–107564GB-I00, PGC2018-099388-BI00, PID2020–114687GB-I00) Government of Andalucia (FQM160, SOMM17/6105/UGR) and the University of Tokyo ICRR's Inter-University Research Program FY2023 Ref. J1, and ERDF funds and CERCA program, Spain; the SNSF and SERI (200021_185012, 200020_188533, 20FL21_186178I), Switzerland; the STFC and UKRI, UK; and the DOE, USA. We also thank CERN for the UA1/NOMAD magnet, DESY for the HERA-B magnet mover system, the BC DRI Group, Prairie DRI Group, ACENET, SciNet, and CalculQuebec consortia in the Digital Research Alliance of Canada, GridPP and the Emerald High Performance Computing facility in the United Kingdom, and the CNRS/IN2P3 Computing Center in France. In addition, the participation of individual researchers and institutions has been further supported by funds from the ERC (FP7), "la Caixa" Foundation (ID 100010434, Fellowship Code No. LCF/BQ/IN17/11620050), the European Union's Horizon 2020 Research and Innovation Programme under the Marie Sklodowska-Curie Grants Agreement No. 713673 and No. 754496, and H2020 Grants No. RISE-GA822070-JENNIFER2 2020 and No. RISE-GA872549-SK2HK; the JSPS, Japan; the Royal Society, UK; French ANR Grant No. ANR-19-CE31-0001; the SNF Eccellenza Grant No. PCEFP2_203261; and the DOE Early Career programme, USA.

[1] B. Pontecorvo, Zh. Eksp. Teor. Fiz. **53**, 1717 (1967).
[2] Z. Maki, M. Nakagawa, and S. Sakata, Prog. Theor. Phys. **28**, 870 (1962).
[3] C. A. Argüelles *et al.*, Eur. Phys. J. C **83**, 15 (2023).
[4] K. Abe *et al.* (The T2K Collaboration), Phys. Rev. D **103**, L011101 (2021).
[5] K. Abe *et al.* (The T2K Collaboration), Phys. Rev. D **96**, 011102 (2017).
[6] K. Abe *et al.* (The T2K Collaboration), Phys. Rev. Lett. **116**, 181801 (2016).
[7] K. Abe *et al.* (The T2K Collaboration), Nucl. Instrum. Methods Phys. Res., Sect. A **659**, 106 (2011).
[8] S. Fukuda *et al.*, Nucl. Instrum. Methods Phys. Res., Sect. A **501**, 418 (2003).
[9] K. Abe *et al.*, Nucl. Instrum. Methods Phys. Res., Sect. A **737**, 253 (2014).
[10] T. Sekiguchi *et al.*, Nucl. Instrum. Methods Phys. Res., Sect. A **789**, 57 (2015).
[11] K. Abe *et al.*, Nucl. Instrum. Methods Phys. Res., Sect. A **694**, 211 (2012).
[12] M. Otani *et al.*, Nucl. Instrum. Methods Phys. Res., Sect. A **623**, 368 (2010).
[13] S. Assylbekov *et al.*, Nucl. Instrum. Methods Phys. Res., Sect. A **686**, 48 (2012).
[14] N. Abgrall *et al.*, Nucl. Instrum. Methods Phys. Res., Sect. A **637**, 25 (2011).
[15] P. A. Amaudruz *et al.* (T2K ND280 FGD Collaboration), Nucl. Instrum. Methods Phys. Res., Sect. A **696**, 1 (2012).
[16] D. Allan *et al.*, J. Instrum. **8**, P10019 (2013).
[17] S. Aoki *et al.*, Nucl. Instrum. Methods Phys. Res., Sect. A **698**, 135 (2013).

[18] M. Jiang *et al.* (The Super-Kamiokande Collaboration), Prog. Theor. Exp. Phys. **2019**, 053F01 (2019).
[19] N. Abgrall *et al.* (The NA61/SHINE Collaboration), Eur. Phys. J. C **76**, 617 (2016).
[20] K. Abe *et al.* (The T2K Collaboration), Phys. Rev. D **103**, 112008 (2021).
[21] K. Abe *et al.* (The T2K Collaboration), Phys. Rev. D **87**, 012001 (2013); **87**, 019902(A) (2013).
[22] N. Abgrall *et al.* (The NA61/SHINE Collaboration), Eur. Phys. J. C **76**, 84 (2016).
[23] K. Abe *et al.* (The T2K Collaboration), Eur. Phys. J. C **83**, 782 (2023).
[24] C. Ahdida *et al.*, Front. Phys. **9**, 788253 (2022).
[25] G. Battistoni *et al.*, Ann. Nucl. Energy **82**, 10 (2015).
[26] Y. Hayato and L. Pickering, Eur. Phys. J. Spec. Top. **230**, 4469 (2021).
[27] C. H. Llewellyn Smith, Phys. Rep. **3**, 261 (1972).
[28] R. Bradford, A. Bodek, H. S. Budd, and J. Arrington, Nucl. Phys. B, Proc. Suppl. **159**, 127 (2006).
[29] O. Benhar, A. Fabrocini, S. Fantoni, and I. Sick, Nucl. Phys. **A579**, 493 (1994).
[30] P. Stowell *et al.*, J. Instrum. **12**, P01016 (2016).
[31] V. Bernard, L. Elouadrhiri, and U.-G. Meissner, J. Phys. G **28**, R1 (2002).
[32] J. Nieves, I. Ruiz Simo, and M. J. Vicente Vacas, Phys. Rev. C **83**, 045501 (2011).
[33] C. Berger and L. M. Sehgal, Phys. Rev. D **76**, 113004 (2007).
[34] K. M. Graczyk and J. T. Sobczyk, Phys. Rev. D **77**, 053001 (2008); **79**, 079903(E) (2009).
[35] M. Gluck, E. Reya, and A. Vogt, Eur. Phys. J. C **5**, 461 (1998).
[36] A. Bodek and U. K. Yang, AIP Conf. Proc. **670**, 110 (2003).
[37] C. Bronner, J. Phys. Soc. Jpn. Conf. Proc. **12**, 010025 (2016).
[38] T. Sjostrand, Comput. Phys. Commun. **82**, 74 (1994).
[39] H. W. Bertini, Phys. Rev. C **6**, 631 (1972).
[40] E. Oset, L. L. Salcedo, and D. Strottman, Phys. Lett. **165B**, 13 (1985).
[41] E. S. Pinzon Guerra *et al.*, Phys. Rev. D **99**, 052007 (2019).
[42] P. Gueye *et al.*, Phys. Rev. C **60**, 044308 (1999).
[43] D. Ruterbories *et al.* (MINERvA Collaboration), Phys. Rev. D **99**, 012004 (2019).
[44] P. A. Rodrigues *et al.* (MINERvA Collaboration), Phys. Rev. Lett. **116**, 071802 (2016); **121**, 209902(A) (2018).
[45] K. Abe *et al.* (The T2K Collaboration), Phys. Rev. D **101**, 112001 (2020).
[46] K. Abe *et al.* (The T2K Collaboration), Phys. Rev. D **101**, 112004 (2020).
[47] J. Nieves, I. Ruiz Simo, and M. J. Vicente Vacas, Phys. Lett. B **707**, 72 (2012).
[48] E. S. Pinzon Guerra *et al.* (DUET Collaboration), Phys. Rev. C **95**, 045203 (2017).
[49] K. Abe *et al.* (The T2K Collaboration), Phys. Rev. D **91**, 072010 (2015).
[50] S. S. Wilks, Ann. Math. Stat. **9**, 60 (1938).
[51] M. Tanabashi *et al.* (Particle Data Group), Phys. Rev. D **98**, 030001 (2018).
[52] The T2K Collaboration, Data release for “Updated T2K measurements of muon neutrino and antineutrino disappearance using 3.6E21 protons on target”, 10.5281/zenodo.7929975 (2023).